ACS OMEGA

Open Access

http://pubs.acs.org/journal/acsodf

Article

Lightweight Flexible and Efficient Electromagnetic Shielding Composites Based on Silver-Coated Glass Microspheres

Rui Xu, Suoxiu Sheng, Changhao Hu, Hangcen Xie, Bin Huang, Pingping Lou, Hua-Feng Fei,* and Zhijie Zhang*

Cite This: *ACS Omega* 2025, 10, 11516−11524

Read Online

ACCESS | Metrics & More | Article Recommendations | Supporting Information

ABSTRACT: Composites consisting of silicone rubber and conductive fillers are extensively utilized in electronic devices due to their high performance in the field of electromagnetic interference (EMI) shielding. Traditional electromagnetic shielding polymer composites often use metal fillers such as silver, which suffer from drawbacks such as high costs and increased density. This study details the synthesis of silver-coated glass microspheres (Ag@GMs) via an ethylene glycol activation method, followed by their application in the formulation of lightweight, flexible, and effective EMI shielding silicone rubber composites. The deposition of a silver coating on the surface of the glass microspheres promotes the constitution of three-dimensional conductive networks, achieving a maximum density of 1.83 g/cm^3 and an electrical conductivity of 204.63 S/cm. At the core−shell interface of the silver-coated glass microspheres, interface polarization loss and the internal reflection of electromagnetic waves are significantly enhanced, resulting in the electromagnetic shielding efficiency of up to 120 dB. Moreover, the composite exhibits excellent bending resistance and aging stability, indicating its promising potential for EMI protection in wearable, smart, and precision electronic applications.

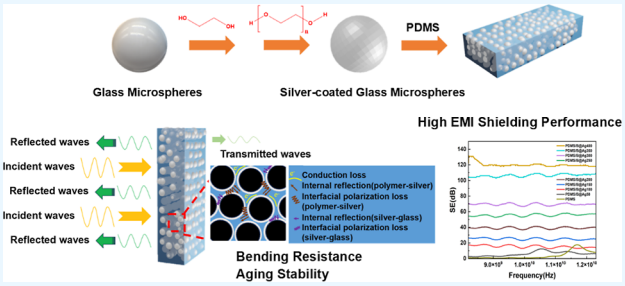

INTRODUCTION

Over the past decades, significant advancements in information technology have coincided with the growing popularity of various consumer electronics, electronic components, sophisticated equipment, and related products.[1−4] The utilization of electromagnetic waves as information carriers has greatly enhanced the transmission of data. However, the uncontrolled proliferation of electromagnetic waves can disrupt the normal functioning of devices and pose risks to human and animal health.[5−7] Consequently, electromagnetic interference (EMI) has garnered considerable attention. Effective management of EMI can be achieved through the reduction of electromagnetic radiation via shielding.[8−12]

As a result, numerous polymer-based EMI shielding composites have been developed, finding diverse applications in aerospace, automotive, and rapidly evolving electronic sectors.[13−16] Nonetheless, these composites often exhibit limitations such as low electromagnetic shielding effectiveness (EMI SE), high density, elevated modulus, and high costs. Additionally, the increasing prevalence of emerging intelligent electronic and wearable devices has amplified the demand for flexible, lightweight, and efficient electromagnetic shielding materials.[17−19] Silicone rubber demonstrates excellent flexibility, radiation resistance, weather resistance, and biocompatibility, making it an essential matrix for the production of flexible functional composites.[20−22]

It is a well-established fact that materials possess high electrical conductivity to achieve optimal EMI SE.[23,24] However, this often necessitates the incorporation of substantial amounts of conductive fillers into the polymer matrix, which can increase manufacturing costs, complicate processing, and elevate material density. The structural design of conductive fillers presents an opportunity to significantly reduce the quantity required while simultaneously enhancing conductivity. Metal-coated core−shell fillers not only demonstrate excellent conductivity but also mitigate the drawbacks associated with the high cost and density of metal materials.[25−27] Because silver has excellent electrical conductivity, it is a commonly used material in the manufacture of EMI shielding composites. Consequently, silver can be deposited on the surface of glass microspheres (GMs) through an electroless plating process, which facilitates the effective distribution of the deposited silver particles and thus enhances the shielding network composed of conductive fillers.[28−30]

Received: January 6, 2025
Revised: February 11, 2025
Accepted: March 6, 2025
Published: March 13, 2025

The introduction of metal particles via electroless plating has garnered significant attention due to its low cost, energy efficiency, simplicity, and effectiveness. But traditional electroless plating processes require complex surface treatments, including sensitization and activation, along with additional procedures. Furthermore, noble metal catalysts have high costs, which limits the broader application of this technique.[31] The use of ethylene glycol for the reduction of silver nitrate-activated materials facilitates high-efficiency activation without the need for coarsening or sensitization, thereby reducing production costs.[32]

In this study, silver-coated glass microspheres (Ag@GMs) were synthesized using ethylene glycol activation. The results indicate that the silver layer is deposited uniformly and densely on the surface of the GMs. Silicone rubber/silver-coated glass microsphere composites (PDMS/Ag@GMs) were prepared using the *n*-hexane solvent method. The unique core−shell structure of the filler enhances the composites' electromagnetic shielding capabilities and electrical conductivity. Additionally, the silicone rubber matrix exhibits favorable flexibility and aging resistance, allowing the composites to maintain exceptional EMI shielding effectiveness even after 400 bends and 3600 h of aging.

EXPERIMENTAL SECTION

Materials. Glass microspheres (>98%) were purchased from Shanxi Hainuo Technology Co., Ltd., acetone (AR) was purchased from Tianjin City Concord Technology Co., Ltd., silver nitrate (>99.8%) was purchased from Sinopharm Chemical Reagent Co., Ltd., ethylene glycol (AR) purchased from Tianjin City Concord Science and Technology Co., Ltd., ammonia (25 wt %) purchased from Xilong Science Co., Ltd., glucose (AR) purchased from Sinopharm Chemical Reagent Co., Ltd., tartaric acid (>99.0%) was purchased from Tokyo Chemical Industry Co., Ltd., hydroxyl-terminated polyethylene glycol (>98%) was purchased from SIGMA-Aldrich, sodium hydroxide (AR) was purchased from Beijing Chemical Plant, and ethanol (AR) was purchased from Tianjin City Concord Technology Co., Ltd., hydroxyl terminated polydimethylsiloxane (5000 mPa·S) was self-made in the laboratory, Tetraethyl silicate (98%) was purchased from Shanghai Maclin Biochemical Technology Co., Ltd., dibutyl tin dilaurate (>96%) was purchased from Beijing Yili Fine Chemicals Co., Ltd., and hexane (GR) was purchased from Tianjin City Concord Technology Co., Ltd.

Preparation of Ag@GMs. A range of glass microsphere (GMs) masses was immersed in a solution of 27.7 g/L silver nitrate in ethylene glycol, subjected to mechanical stirring under ultrasonic agitation for several hours (Table 1). The resulting suspension was then centrifuged to separate the precipitate, which was subsequently washed three times with deionized water and twice with ethanol. Eventually, the samples were vacuum-dried at 60 °C for 4 h, yielding the desired products, designated as A-GMs.

Table 1. Reaction Conditions for Different Activated GMs[a]

	amount of GMs (g/L)	activation time (h)
(1)	50/75/100/125	18
(2)	75	6/12/18/24

[a]The concentration of silver nitrate in ethylene glycol solution of each group was 27.7 g/L.

The solution was prepared by means of the dissolution of 3.0 g of silver nitrate in 17.22 mL of deionized water, followed by the dropwise addition of ammonia. Initially, a brownish precipitate formed in the solution, and stirring was continued until the precipitate dissolved completely. The dropwise addition of ammonia was then halted to obtain a silver−ammonia complex solution. Subsequently, a reducing solution was prepared by heating a mixture of 6.32 g of glucose and 0.64 g of tartaric acid in 287.5 mL of deionized water and 28.75 mL of ethanol to boiling for 15 min. This solution was then cooled and utilized as the reducing agent.

A-GMs of varying mass were dispersed in a reducing solution, 0.06 g of polyethylene glycol was added, mechanical stirring was performed under ultrasonic action for 0.5 h, NaOH was added to adjust pH, and a silver ammonia solution prepared beforehand was added dropwise to the solution. Subsequently, the mixture was then subjected to a reaction in an oil bath at various temperatures for a period of several hours, as detailed in Table 2. The mixture was subjected to centrifugation to separate the precipitate, which was then washed on three occasions with deionized water and twice with ethanol. Ultimately, vacuum drying at 60 °C for 4 h yielded the desired samples, designated Ag@GMs.

Table 2. Preparation Conditions of Different Ag@GMs

	amount of A-GMs (g/L)	reaction time (h)	reaction temperature (°C)	pH
(1)	5/15/25/35	6	25	11
(2)	15	2/4/6/8	25	11
(3)	15	6	15/25/35/45	11
(4)	15	6	25	10/11/12/13

Preparation of PDMS/Ag@GMs. A quantity of 5.0 g of silver-coated glass microspheres was weighed and immersed in 100 mL of *n*-hexane. The solution was mechanically stirred to ensure even dispersion, resulting in component 1. Concurrently, 10 g of hydroxy-terminated polydimethylsiloxane (PDMS) was weighed and dissolved in 50 mL of *n*-hexane, serving as component 2.

Components 1 and 2 were combined and subjected to magnetic stirring for 0.5 h following a 0.5 h sonication process. The mixture was then concentrated to approximately 50 mL using rotary evaporation, and the hexane solvent was subsequently evaporated by heating to 50 °C for 12 h under a nitrogen atmosphere.

Following this, the mixture underwent vacuum drying at 40 °C for 24 h to remove residual hexane solvent. Subsequently, 3−5% tetraethyl silicate and 0.5−1% dibutyl tin dilaurate were added and mixed uniformly. The resulting mixture was transferred to a specialized mold and subjected to bubble discharge treatment. The mixture was subsequently permitted to stand at ambient temperature for 24 h, thereby completing the curing process (Figure S1).

Characterization. X-ray diffractometers (XRD, Empyrean, Panaco) were employed to corroborate the deposition of silver particles on the surface of glass microspheres, as well as the activation and electroless plating of the glass microspheres. The micromorphology of the glass microspheres was observed using a field emission scanning electron microscope (SEM, SU8020, Hitachi, Japan). A semiconductor characterization tester (Scs-4200, Keithley Instruments, Inc.) is employed for the measurement of electrical conductivity in composite

https://doi.org/10.1021/acsomega.5c00148
ACS Omega 2025, 10, 11516−11524

materials. The test samples are formed into dumbbell-shaped structures (Figure S2). Thermal conductivity tests are conducted using thermal conductivity testers (TCI, C-Therm) (Figure S3). The electromagnetic interference (EMI) shielding performance scattering parameters (S_{11} and S_{21}) of the samples (Figure S4) were evaluated using a vector network analyzer (VNA) (E5071C, Keysight Technology Co) and a straight waveguide (HD-100WAL100, Xian Hengda Microwave Technology Development Co., Ltd.) (Figure S5). The reflected power coefficient (R), transmission power coefficient (T), absorbed power coefficient (A), reflected electromagnetic shielding effectiveness (SER), absorbed electromagnetic shielding effectiveness (SEA) and total electromagnetic shielding effectiveness (SET) were calculated using a VNA (Keysight Technology Co., Ltd.) in the X-band frequency range (8.2−12.4 GHz).[29,33,34] Detailed calculation process is outlined in Formulas 1−6 in the Supporting Information. After the test sample is made into a dumbbell specimen (Figure S2), the specimen is tested using a universal tensile tester (Instron 5565, Inc., USA) testing. The hardness of composite materials is evaluated through the utilization of a rubber hardness tester (LX-A, Shanghai Liuling Instrument Factory).

RESULTS AND DISCUSSION

Morphology and Phase Characterization of GMs,A-GMs and Ag@GMs. Figure 1a presents scanning electron microscopy (SEM) images of glass microspheres (GMs), characterized by a regular spherical shape, a smooth surface, and minimal impurity presence. Figure 1b displays an SEM image of A-GMs, revealing a uniform layer of nanosized silver particles generated on the surface. These silver nanoparticles serve as nucleation centers, facilitating the deposition of reduced silver during the electroless plating process. Upon the addition of the silver ammonia solution, a color change from dark brown to light gray (Figure S6) was observed, indicating that an in situ chemical reduction reaction had occurred on the surface of the A-GMs. Figure 1c shows an SEM image of Ag@GMs, where a uniform and complete layer of silver nanoparticles is deposited on the surface. Compared with A-GMs, the particle diameter increased significantly. The results demonstrate that substantial quantities of silver deposit on the surface of A-GMs during electroless plating, forming a dense and uniform silver layer, which yields Ag@GMs with a pronounced core−shell structure. A comparison of the X-ray diffraction (XRD) patterns (Figure 1d) for GM, A-GMs, and Ag@GMs reveals that the signal intensity for A-GMs is weaker due to the smaller size and lower total amount of silver particles. The XRD pattern for Ag@GMs exhibits five characteristic peaks at 38.20, 44.40, 64.60, 77.50, and 81.60°, corresponding to the diffraction crystal planes (111), (200), (220), (311), and (222), respectively. These crystallographic characteristics of silver align well with the standard data from JCPDS 89-3722, confirming that the glass microspheres have been successfully coated with a silver layer.[26,35]

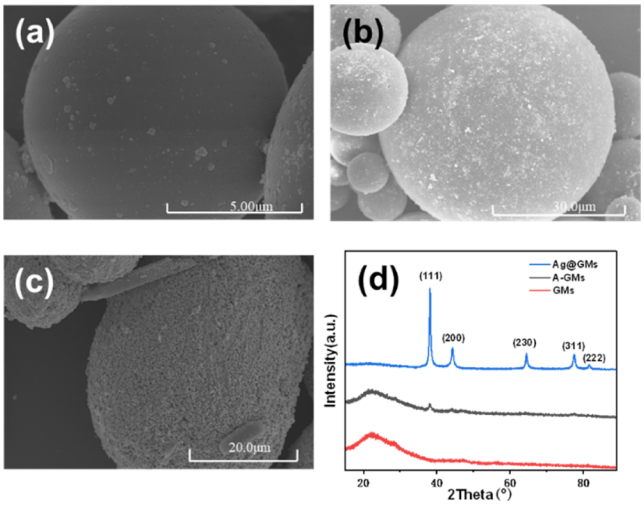

Figure 1. (a) SEM images of GMs; (b) SEM images of A-GMs obtained by 75 g/L GMs and activation for 18 h; (c) SEM images of Ag@GMs obtained by 15 g/L A-GMs ,pH 11 at 25 °C and reaction for 6 h; (d) XRD images of GMs, A-GMs and Ag@GMs.

The activation of the material's surface is a critical stage in the electroless silver plating process, aimed at generating a specific quantity of silver nuclei on the surface to initiate silver deposition. A comparative analysis of SEM images of A-GMs prepared under different activation conditions (Table 1) revealed a significant reduction in silver particle density on the surface of A-GMs with increasing GMs dosage. A-GMs produced under conditions of 50 g/L (Figure 2a1) and 75 g/L (Figure 1b) exhibited greater uniformity and completeness in silver particle coverage. As the quantity of GMs increases, the available surface area for plating also increases, while the total amount of silver deposited remains constant. This results in a decreased density of silver particles on the surface of A-GMs, ultimately leading to insufficient uniform coverage of the microspheres (Figure 2a2,a3). Figure 2b1−b3 illustrate SEM images of A-GMs obtained at varying activation times. At an activation time of 6 h (Figure 2b1), the degree of reaction is low, with a significant amount of silver nitrate remaining unreacted and only a modest quantity of silver particles deposited on the surface of the GMs. As the reaction time is extended, a larger proportion of silver nitrate participates in the reaction, resulting in increased silver particle coverage on the GMs. The silver particles on the surface of A-GMs obtained after 18 h of reaction time (Figure 1b) are observed to be more densely packed. However, the concentration of silver nitrate in the solution decreases markedly, the reaction rate slows significantly, and the density of silver particles on the surface of GMs remains relatively unchanged, as the reaction time is extended to 24 h. These findings demonstrate that the encapsulation of silver particles on the surface of A-GMs can be controlled by varying both the dosage of GMs and the activation reaction time. The final optimized activation conditions were established at 18 h with a GM concentration of 75 g/L, which were utilized for subsequent studies.

Figure 3 shows SEM images of Ag@GMs obtained under varying reaction conditions, as detailed in Table 2. The addition of 5 g/L of activated glass microspheres results in a reduction in the number of nucleation centers, coupled with an increase in the quantity of silver ions associated with each nucleation center. This leads to an enhanced crystal growth rate and the formation of a substantial amount of flake silver on the surface of the glass microspheres (Figure 3a1). At a dosage of 15 g/L, silver is deposited as nanoparticles on the surface of the glass microspheres, resulting in a uniform and dense silver layer (Figure 1c). However, as the dosage of A-GMs is increased further, the available surface area for silver deposition also increases, leading to a decrease in the density of silver

https://doi.org/10.1021/acsomega.5c00148
ACS Omega 2025, 10, 11516−11524

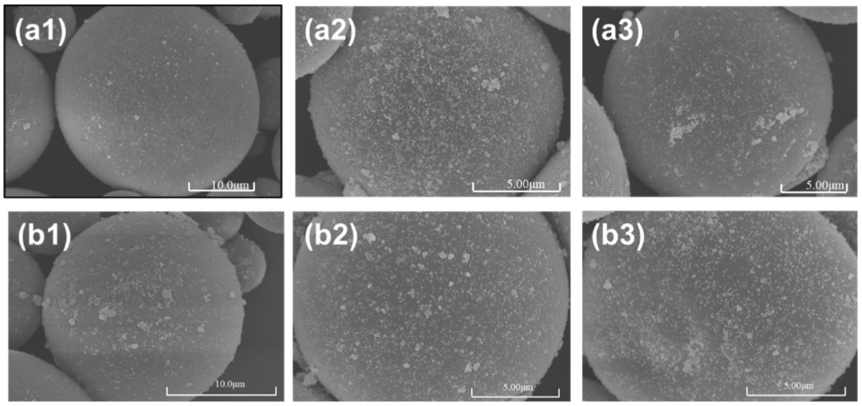

Figure 2. SEM images of A-GMs obtained under different activation conditions; (a1−a3) SEM images of A-GMs obtained when GMs dosage is 50/100/125 g/L; (b1−b3) SEM images of A-GMs obtained when activation time is 6/12/24 h.

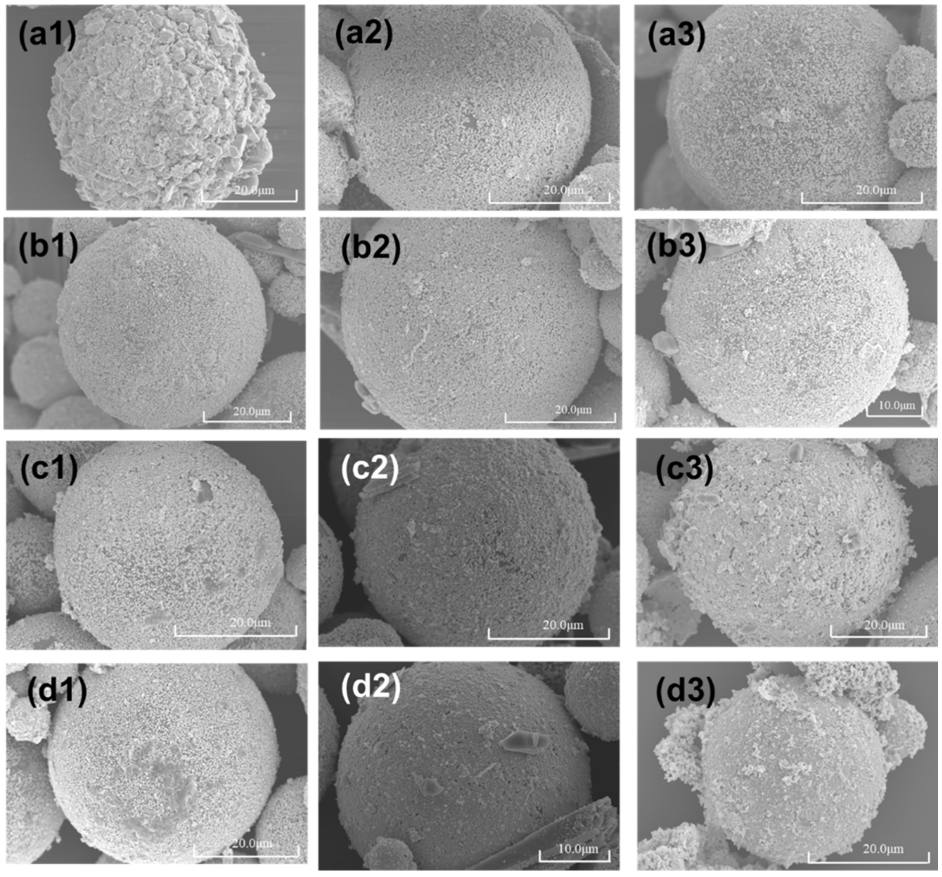

Figure 3. SEM images of Ag@GMs obtained under different reaction conditions; SEM images of Ag@GMs obtained when (a1−a3) A-GMs dosage is 5/25/35 g/L; SEM images of Ag@GMs obtained when (b1−b3) reaction time is 2/4/8 h; SEM images of Ag@GMs obtained when (c1−c3) reaction temperature is 15/35/45 °C; SEM images of Ag@GMs obtained when (d1−d3) plating solution pH is 10/12/13.

particles on the microsphere surfaces. Consequently, the silver coating becomes loose and uneven (Figure 3a2,a3). This indicates that the dosage of GMs significantly influences the activation effect during the same activation process; both excess and insufficient amounts of A-GMs adversely affect the formation of a high-quality silver coating. Therefore, the optimal dosage of A-GMs was determined to be 15 g/L.

Figure 3b1−b3 illustrate the silver coating morphology of Ag@GMs obtained at varying reaction times (2, 4, and 8 h). At a reaction time of 2 h, the silver particles on the surface of Ag@GMs are relatively small and sparsely distributed, making it challenging to form a macroscopic silver layer (Figure 3b1). This is attributed to insufficient reaction time and a low degree of reaction, preventing a significant number of silver ions in the solution from undergoing reduction. As the reaction time is extended, the degree of reaction increases, resulting in larger particle size and higher density of silver particles on the microspheres, gradually forming a dense and uniform silver layer (Figures 1c, 2 and 3b2). However, upon extending the reaction time further, distinct undulations and defects appear on the surface of the silver layer, contrasting with the gradual and gentle activation reaction in ethylene glycol. Additionally,

https://doi.org/10.1021/acsomega.5c00148
ACS Omega 2025, 10, 11516−11524

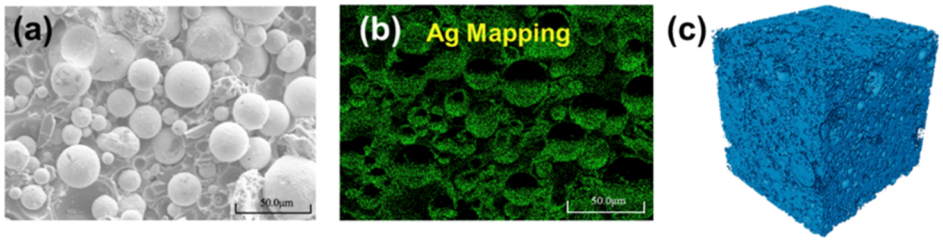

Figure 4. (a) SEM image of PDMS/Ag@GMs cross section; (b) the corresponding element mapping; (c) PDMS/Ag@GMs computer tomography simulation results.

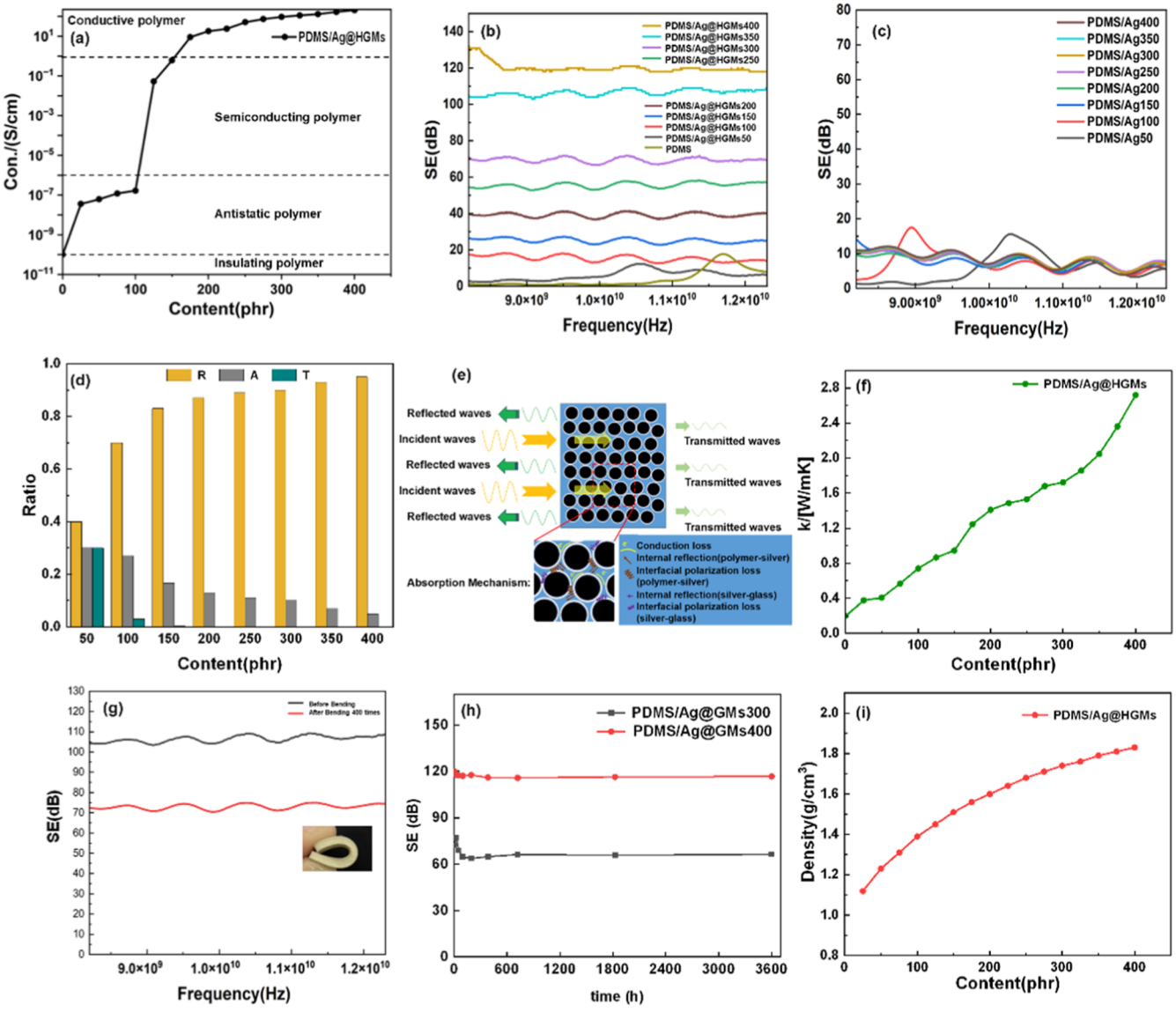

Figure 5. (a) Change trend of conductivity of PDMS/Ag@GMs with different Ag@GMs addition; (b) EMI SE of PDMS/Ag@GMs with different filler content in X-band; (c) EMI SE of silicone rubber/silver powder composite (PDMS/Ag); (d) analysis of transmittance (T), reflectivity (R) and absorptivity (A) of PDMS/Ag@GMs by electromagnetic wave; (e) analysis of electrical shielding mechanism of PDMS/Ag@GMs; (f) change trend of thermal conductivity of PDMS/Ag@GMs with filler addition; (g) EMI SE change in X-band of PDMS/Ag@GMs material (350 filling) after 400 bending cycles; (h) EMI SE of Ag@GMs after aging at 125 °C; (i) density change trend of PDMS/Ag@GMs material with filling fraction.

a considerable amount of free silver is observed (Figure 3b3). This phenomenon occurs because, after approximately 6 h of reaction, the reaction is nearly complete. During the subsequent reaction time, disturbances caused by ultrasonic stirring can damage the silver coating, leading to detachment of the silver layer and the formation of free silver. Consequently, the optimal reaction time was determined to be 6 h.

Figure 3c1−c3 illustrate the impact of varying reaction temperatures (15, 35, and 45 °C) on the morphology of the silver layer. At insufficient temperatures, the reaction proceeds sluggishly, resulting in smaller silver particles and lower

https://doi.org/10.1021/acsomega.5c00148
ACS Omega 2025, 10, 11516−11524

deposition density (Figure 3c1). As the temperature increases, the deposition rate of silver rises, leading to a deeper degree of reaction and a gradual enhancement in the deposition density of silver particles on the surface of the glass microspheres (Figure 1c). At the reaction temperature of 35 °C, a notable amount of free silver is observed in the solution (Figure 3c2). However, when the temperature is further increased to 45 °C, the reaction speed becomes excessively rapid, causing a significant precipitation of silver ions as free silver. This results in a marked increase in the particle size of silver particles, with considerable accumulation and highly uneven distribution (Figure 3c3). Consequently, the optimal reaction temperature was determined to be 25 °C.

Figure 3 illustrates the impact of pH on coating morphology, with images d1, d2, and d3 providing a visual representation of this effect. The SEM images reveal that at lower pH values, the silver particle size is relatively small, and the particle size distribution is more uniform (Figure 3d1). As the pH value increases, the silver particle size and the amount of free silver produced also increase (Figure 3d3). This phenomenon can be attributed to two main factors. First, an increase in pH accelerates the reaction rate, resulting in a corresponding increase in the particle size of silver particles. Second, ammonia acts as a complexing agent, capturing silver ions in solution. However, at elevated pH levels, the solution tends to self-decompose, resulting in the production of free silver. To prevent deterioration in the density of the silver layer and excessive free silver formation, it is recommended that the pH of the plating solution be maintained at 11.

Characterization of PDMS/Ag@GMs. The cross-sectional SEM images of PDMS/Ag@GMs (Figure 4a) reveal that the Ag@GMs are effectively dispersed within the PDMS matrix, exhibiting minimal agglomeration. Energy-dispersive spectroscopy (EDS) was utilized to observe the element distribution of the particle coating (Figures 4b, S7 and S8). Following the composite preparation process, it was observed that the silver coating on the surface of Ag@GMs remained intact and dense. The computed tomography simulation results (Figure 4c) indicate that the Ag@GMs are uniformly distributed throughout the composite, demonstrating close contact with one another and forming a connected three-dimensional conductive network via the interaction of the surface silver layer (Figure S9).

Conducting and Electromagnetic Shielding Properties of PDMS/Ag@GMs. As conductivity is the primary parameter for assessing the efficacy of EMI shielding, first, we evaluated the conductivity of PDMS/Ag@GMs. Figure 5a illustrates the variation in conductivity of PDMS/Ag@GMs with differing amounts of Ag@GMs. Upon increasing the addition from 100 to 150 phr, a notable increase in conductivity was observed, rising from 10^{-7} to 10^{-1} S/cm. This increase can be attributed to the attainment of the percolation threshold within the filled system at this specific point. When the Ag@GMs content reaches 100 phr, a greater number of contact points emerge between the particles, facilitating the construction of three-dimensional conductive pathways. Further increasing the addition to 200 phr results in conductivity rising to 8.93 S/cm, a level comparable to that of conductive polymers (exceeding 1 S/cm).[36] As the filler content increases, the conductivity of the composites stabilizes, as the conductive pathways have been sufficiently established, making conductivity less sensitive to further increases in filler content. At 400 phr, the conductivity reaches 204.63 S/cm, demonstrating excellent conductivity.

Figure 5b shows the electromagnetic interference EMI SE of PDMS/Ag@GMs with varying filler contents in the X-band frequency range. EMI SE gradually increases with the amount of filler, particularly after reaching the percolation threshold. At the highest filler content, the EMI SE achieves an impressive 120 dB, indicating that 99.999999% of electromagnetic waves can be effectively shielded. This exceptional EMI SE value positions PDMS/Ag@GMs as a highly competitive option among practical electromagnetic shielding materials.

To demonstrate the efficacy of constructing three-dimensional conductive pathways using silver layers on the surface of GMs, we investigated the EMI SE of rubber composites with nanosilver powder as a conductive filler (PDMS/Ag) at the same addition level (Figure 5c). At a content of 400 phr of Ag, the EMI SE is approximately 10 dB. In contrast, when the PDMS/Ag@GMs content reaches 400 phr, the EMI SE increases significantly to 120 dB, indicating a high degree of filling efficiency for PDMS/Ag@GMs. This difference can be attributed to the high density of the nanosilver powder, which hinders the formation of efficient conductive pathways. Conversely, the silver-coated glass microspheres are lightweight,[37,38] and their higher volume fraction in the same proportion facilitates the development of conductive paths within the composites.

To gain insight into the electromagnetic shielding mechanism of the materials, we analyzed the reflection and absorption of electromagnetic signals (Figure 5d). As the filler content increases, the electromagnetic wave transmittance (T) of the composites continuously declines, consistent with the observed enhancement in electromagnetic shielding effectiveness. At a filler content of 400 phr, the electromagnetic wave transmittance of the composites is approximately 10^{-12}. With increasing additive amounts, the reflectivity continues to rise. This occurs because when an incident electromagnetic wave encounters the shielding material, it is first affected by the material's reflection shielding effect. The reflection shielding effectiveness directly influences the reflectivity. When the filler content reaches 300 phr, the reflectivity exceeds 90%. Conversely, absorptivity declines as reflectivity increases, because the increase in reflectivity decreases the energy of the electromagnetic wave that passes through the surface and enters the interior. This effect is more pronounced than the enhancement of absorption shielding effectiveness. Therefore, we can conclude that the material primarily operates as an electromagnetic shielding material with a reflective mechanism.

Figure 5e illustrates the electrical shielding mechanism of PDMS/Ag@GMs. These composites exhibit excellent conductivity properties. When electromagnetic waves interact with the material surface, a part of the wave is reflected by the highly conductive surface, while the remainder penetrates the material and is subsequently attenuated through reflection and absorption. The incorporation of silver-coated glass microspheres into the matrix leads to the formation of silicone rubber-silver and silver-glass microscopic interfaces within the system. These microscopic interfaces produce two distinct effects on electromagnetic waves. First, interface relaxation loss occurs, resulting in the absorption of some energy. Second, reflection at these microscopic interfaces increases the path length of the electromagnetic waves traveling through the material, enhancing their absorption. This explains the phenomenon where the material's conductivity gradually

https://doi.org/10.1021/acsomega.5c00148
ACS Omega 2025, 10, 11516−11524

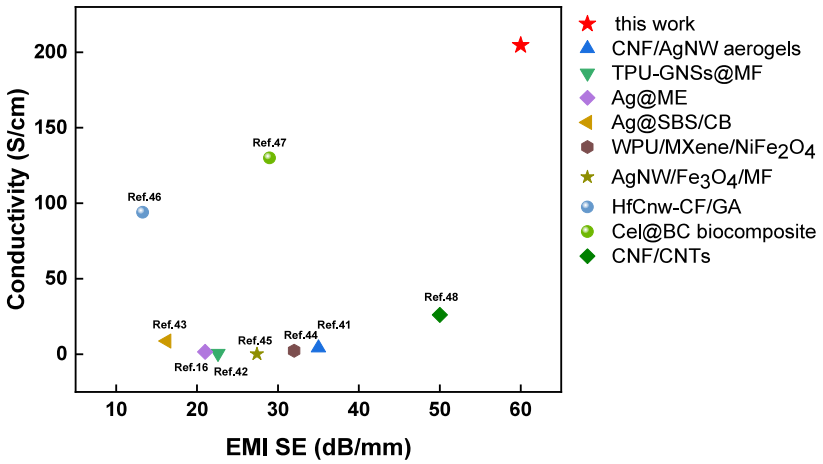

Figure 6. Comparison of EMI SE and bulk conductivity of the EMI shielding materials.

increases while the EMI SE markedly improves at higher filler concentrations. The continuous enhancement of interface relaxation loss and internal reflection effects due to the increased quantity of silver-coated glass microspheres significantly boosts the EMI SE of the composites.

Figure 5f illustrates the trend in thermal conductivity of the PDMS/Ag@GMs material with filler additions. The three-dimensional conductive pathways within the material facilitate heat conduction through an electronic thermal conduction mechanism.[39,40] Consequently, thermal conductivity increases in proportion to the number of filler particles present. When the filler content is 400 parts, the thermal conductivity of the material is observed to be 2.72 W/(m·K). In addition, Ag@GMs are rigid fillers and have a certain reinforcement effect on PDMS matrix (Figure S11a). At the same time, the elongation at break of the composites decreases with the increase of filler content due to the poor interfacial compatibility between silver layer and PDMS matrix. When the filler content is 400 phr, the tensile strength of the composites is 1.18 MPa (Figure S11b), and the elongation at break is 10% (Figure S11c).

To provide a more intuitive representation of the thermal conductivity, the PDMS matrix material and the PDMS/Ag@GMs (with 400 phr filled) were puted on a hot table. The temperature of PDMS/Ag@GMs is obviously higher than that of pure PDMS, while they are heated simultaneously, it shows that PDMS/Ag@GMs has excellent thermal conductivity. This observation further substantiates the superior thermal conductivity of the composites (Figure S10).

The bending fatigue resistance of EMI shielding materials is a critical factor in determining its practical application. Consequently, bending fatigue testing was conducted to assess the reliability of EMI SE in PDMS/Ag@GMs. Figure 5g shows that 2 mm thick PDMS/Ag@GMs (with 350 phr filled) exhibit remarkable resilience to bending fatigue, retaining excellent electromagnetic shielding properties with EMI SE values as high as 73 dB in the X-band after 400 bending cycles. Additionally, PDMS/Ag@GMs demonstrate exceptional resistance to aging effects. As shown in Figure 5h, the EMI SE of the material, following exposure to 125 °C for 3600 h, shows minimal change compared to its preaging performance. Furthermore, the density of PDMS/Ag@GMs is less than 1.83 g/cm^3 (Figure 5i), meeting the criteria for lightweight and flexible electromagnetic shielding materials. Moreover, PDMS/Ag@GMs exhibit superior EMI SE and bulk conductivity compared to other reported composites (Figure 6).[16,41−48] This suggests their potential applications in diverse fields, including wearable electronics, artificial intelligence, and 5G communications.

CONCLUSION

A method for preparing silver-coated glass microspheres via ethylene glycol activation is presented. This activation process is highly efficient, cost-effective, and straightforward. The resulting silver-coated glass microspheres feature a compact and uniform coating. The density of the silicone rubber/silver-coated glass microsphere composite material prepared with these microspheres is less than 1.83 g/cm^3. With a thickness of only 2 mm, the corresponding X-band EMI SE can reach 120 dB, and the conductivity is measured at 204.63 S/cm. Moreover, the material exhibits excellent flexibility, resistance to aging, and stability concerning electromagnetic interference shielding effectiveness. This work offers a viable methodology for fabricating lightweight, flexible, and effective electromagnetic shielding materials, presenting promising applications in electronic equipment and devices.

ASSOCIATED CONTENT

Supporting Information

The Supporting Information is available free of charge at https://pubs.acs.org/doi/10.1021/acsomega.5c00148.

The additional synthesis details and characterizations (PDF)

AUTHOR INFORMATION

Corresponding Authors

Hua-Feng Fei − *Key Laboratory of Science and Technology on High-tech Polymer Materials, Institute of Chemistry, Chinese Academy of Sciences, Beijing 100190, P. R. China; School of Chemical Sciences, University of Chinese Academy of Sciences, Beijing 100049, P. R. China;* orcid.org/0000-0002-9983-2725; Email: feihuafeng@iccas.ac.cn

Zhijie Zhang − *Key Laboratory of Science and Technology on High-tech Polymer Materials, Institute of Chemistry, Chinese Academy of Sciences, Beijing 100190, P. R. China;* Email: zhangzj@iccas.ac.cn

https://doi.org/10.1021/acsomega.5c00148
ACS Omega 2025, 10, 11516−11524

Authors

Rui Xu − *Key Laboratory of Science and Technology on High-tech Polymer Materials, Institute of Chemistry, Chinese Academy of Sciences, Beijing 100190, P. R. China; School of Chemical Sciences, University of Chinese Academy of Sciences, Beijing 100049, P. R. China*

Suoxiu Sheng − *Shenyang Aircraft Design Institute of Aviation Industry Corporation of China, Shenyang 110035, P. R. China*

Changhao Hu − *Key Laboratory of Science and Technology on High-tech Polymer Materials, Institute of Chemistry, Chinese Academy of Sciences, Beijing 100190, P. R. China; School of Chemical Sciences, University of Chinese Academy of Sciences, Beijing 100049, P. R. China*

Hangcen Xie − *Key Laboratory of Science and Technology on High-tech Polymer Materials, Institute of Chemistry, Chinese Academy of Sciences, Beijing 100190, P. R. China; School of Chemical Sciences, University of Chinese Academy of Sciences, Beijing 100049, P. R. China*

Bin Huang − *Key Laboratory of Science and Technology on High-tech Polymer Materials, Institute of Chemistry, Chinese Academy of Sciences, Beijing 100190, P. R. China*

Pingping Lou − *Key Laboratory of Science and Technology on High-tech Polymer Materials, Institute of Chemistry, Chinese Academy of Sciences, Beijing 100190, P. R. China*

Complete contact information is available at: https://pubs.acs.org/10.1021/acsomega.5c00148

Notes

The authors declare no competing financial interest.

■ ACKNOWLEDGMENTS

The Analytical Instrumental Center for Physicochemical Analysis and Measurements, Chinese Academy of Sciences supported facilities used in this work.

■ REFERENCES

(1) Nan, Z.; Wei, W.; Lin, Z.; Chang, J.; Hao, Y. Flexible Nanocomposite Conductors for Electromagnetic Interference Shielding. *Nano-Micro Lett.* **2023**, *15* (1), 172.

(2) Kim, T.; Pak, S.; Lim, J.; Hwang, J. S.; Park, K. H.; Kim, B. S.; Cha, S. Electromagnetic Interference Shielding with 2D Copper Sulfide. *ACS Appl. Mater. Interfaces* **2022**, *14* (11), 13499−13506.

(3) Doshi, P.; Wong, H. Y.; Gutierrez, D. H.; Lopez, A.; Nordlund, D.; Gandhiraman, R. P. Printing of electromagnetic interference shielding materials. *Flexible Printed Electron.* **2023**, *8* (2), 025003.

(4) Xie, Y. D.; Liu, S.; Huang, K. W.; Chen, B. B.; Shi, P. C.; Chen, Z. L.; Liu, B. Z.; Liu, K. H.; Wu, Z. Q.; Chen, K.; Qi, Y.; Liu, Z. F. Ultra-Broadband Strong Electromagnetic Interference Shielding with Ferromagnetic Graphene Quartz Fabric. *Adv. Mater.* **2022**, *34* (30), 2202982.

(5) Devi, N.; Ray, S. S. Electromagnetic interference cognizance and potential of advanced polymer composites toward electromagnetic interference shielding: A review. *Polym. Eng. Sci.* **2022**, *62* (3), 591−621.

(6) Jia, Z. X.; Zhang, M. F.; Liu, B.; Wang, F. C.; Wei, G.; Su, Z. Q. Graphene Foams for Electromagnetic Interference Shielding: A Review. *ACS Appl. Nano Mater.* **2020**, *3* (7), 6140−6155.

(7) Wang, N. N.; Zou, W. H.; Li, X. Y.; Liang, Y. Q.; Wang, P. Study and application status of the nonthermal effects of microwaves in chemistry and materials science - a brief review. *RSC Adv.* **2022**, *12* (27), 17158−17181.

(8) Guo, H. T.; Chen, Y. M.; Li, Y.; Zhou, W.; Xu, W. H.; Pang, L.; Fan, X. M.; Jiang, S. H. Electrospun fibrous materials and their applications for electromagnetic interference shielding: A review. *Composites, Part A* **2021**, *143*, 106309.

(9) Sarkar, B.; Miquet-Westphal, F.; Bobbara, S.; George, B.; Beltrame, G.; Dousset, D.; Wu, K.; Cicoira, F. Electromagnetic interference shielding in lightweight carbon xerogels. *Mater. Res. Express* **2023**, *10* (4), 045601.

(10) Kumar, P. Ultrathin 2D Nanomaterials for Electromagnetic Interference Shielding. *Adv. Mater. Interfaces* **2019**, *6* (24), 1901454.

(11) Han, M. K.; Shuck, C. E.; Rakhmanov, R.; Parchment, D.; Anasori, B.; Koo, C. M.; Friedman, G.; Gogotsi, Y. Beyond $Ti_3C_2T_x$: MXenes for Electromagnetic Interference Shielding. *ACS Nano* **2020**, *14* (4), 5008−5016.

(12) Hong, G. H.; Qu, Q.; Rojas, O. J.; Li, L.; Xie, D. L.; Liu, Y. X. Epiphyte-inspired multifunctional biocomposites for electromagnetic interference shielding. *Chem. Eng. J.* **2023**, *469*, 143960.

(13) Li, J.; Wang, Y.; Yue, T. N.; Gao, Y. N.; Shi, Y. D.; Shen, J. B.; Wu, H.; Wang, M. Robust electromagnetic interference shielding, joule heating, thermal conductivity, and anti-dripping performances of polyoxymethylene with uniform distribution and high content of carbon-based nanofillers. *Compos. Sci. Technol.* **2021**, *206*, 108681.

(14) Kong, D. Y.; Li, J.; Guo, A. R.; Xiao, X. L. High temperature electromagnetic shielding shape memory polymer composite. *Chem. Eng. J.* **2021**, *408*, 127365.

(15) Shukla, V.; Srivastava, S. K. Reduced graphene oxide/PdNi/poly(ethylene-co-vinyl acetate) nanocomposites for electromagnetic interference shielding. *Mater. Chem. Phys.* **2022**, *276*, 125418.

(16) Liao, S. Y.; Li, G.; Wang, X. Y.; Wan, Y. J.; Zhu, P. L.; Hu, Y. G.; Zhao, T.; Sun, R.; Wong, C. P. Metallized Skeleton of Polymer Foam Based on Metal-Organic Decomposition for High-Performance EMI Shielding. *ACS Appl. Mater. Interfaces* **2022**, *14* (2), 3302−3314.

(17) Zhang, Z. T.; Wang, W. C.; Jiang, Y. W.; Wang, Y. X.; Wu, Y. L.; Lai, J. C.; Niu, S. M.; Xu, C. Y.; Shih, C. C.; Wang, C.; Yan, H. P.; Galuska, L.; Prine, N.; Wu, H. C.; Zhong, D. L.; Chen, G.; Matsuhisa, N.; Zheng, Y.; Yu, Z. A.; Wang, Y.; Dauskardt, R.; Gu, X. D.; Tok, J. B. H.; Bao, Z. N. High-brightness all-polymer stretchable LED with charge-trapping dilution. *Nature* **2022**, *603* (7902), 624.

(18) Liu, Y. H.; Shen, S.; Hu, J.; Chen, L. S. Embedded Ag mesh electrodes for polymer dispersed liquid crystal devices on flexible substrate. *Opt. Express* **2016**, *24* (22), 25774−25784.

(19) Zhao, H.; Huang, Y. S.; Yun, J.; Wang, Z. Y.; Han, Y. C.; Zheng, Y. P.; Chen, L. X. Stretchable polymer composite film based on pseudo-high carbon-filler loadings for electromagnetic interference shielding. *Composites, Part A* **2022**, *157*, 106937.

(20) Guo, Y. Q.; Qiu, H.; Ruan, K. P.; Wang, S. S.; Zhang, Y. L.; Gu, J. W. Flexible and insulating silicone rubber composites with sandwich structure for thermal management and electromagnetic interference shielding. *Compos. Sci. Technol.* **2022**, *219*, 109253.

(21) Prasad, R.; Pai, A. R.; Oyadiji, S. O.; Thomas, S.; Parashar, S. K. S. Utilization of hazardous red mud in silicone rubber/MWCNT nanocomposites for high performance electromagnetic interference shielding. *J. Cleaner Prod.* **2022**, *377*, 134290.

(22) Liu, D.; Kong, Q. Q.; Jia, H.; Xie, L. J.; Chen, J. P.; Tao, Z. C.; Wang, Z.; Jiang, D.; Chen, C. M. Dual-functional 3D multi-wall carbon nanotubes/graphene/silicone rubber elastomer: Thermal management and electromagnetic interference shielding. *Carbon* **2021**, *183*, 216−224.

(23) Chen, J.; Liao, X.; Xiao, W.; Yang, J. M.; Jiang, Q. Y.; Li, G. X. Facile and Green Method To Structure Ultralow-Threshold and Lightweight Polystyrene/MWCNT Composites with Segregated Conductive Networks for Efficient Electromagnetic Interference Shielding. *ACS Sustainable Chem. Eng.* **2019**, *7* (11), 9904−9915.

(24) Yang, J. M.; Liao, X.; Wang, G.; Chen, J.; Tang, W. Y.; Wang, T. F.; Li, G. X. Fabrication of lightweight and flexible silicon rubber foams with ultra-efficient electromagnetic interference shielding and adjustable low reflectivity. *J. Mater. Chem. C* **2020**, *8* (1), 147−157.

(25) Panahi-Sarmad, M.; Noroozi, M.; Abrisham, M.; Eghbalinia, S.; Teimoury, F.; Bahramian, A. R.; Dehghan, P.; Sadri, M.; Goodarzi, V. A Comprehensive Review on Carbon-Based Polymer Nanocomposite

Foams as Electromagnetic Interference Shields and Piezoresistive Sensors. *ACS Appl. Electron. Mater.* **2020**, *2* (8), 2318−2350.
(26) Yang, J. M.; Liao, X.; Wang, G.; Chen, J.; Guo, F. M.; Tang, W. Y.; Wang, W.; Yan, Z. H.; Li, G. X. Gradient structure design of lightweight and flexible silicone rubber nanocomposite foam for efficient electromagnetic interference shielding. *Chem. Eng. J.* **2020**, *390*, 124589.
(27) Yang, J. M.; Liao, X.; Wang, G.; Chen, J.; Song, P. W.; Tang, W. Y.; Guo, F. M.; Liu, F.; Li, G. X. Heterogeneous silicon rubber composite foam with gradient porous structure for highly absorbed ultra-efficient electromagnetic interference shielding. *Compos. Sci. Technol.* **2021**, *206*, 108663.
(28) Yang, J. M.; Yang, Y. Q.; Duan, H. J.; Zhao, G. Z.; Liu, Y. Q. Light-weight epoxy/nickel coated carbon fibers conductive foams for electromagnetic interference shielding. *J. Mater. Sci.:Mater. Electron.* **2017**, *28* (8), 5925−5930.
(29) Kim, D. G.; Choi, J. H.; Choi, D. K.; Kim, S. W. Highly Bendable and Durable Transparent Electromagnetic Interference Shielding Film Prepared by Wet Sintering of Silver Nanowires. *ACS Appl. Mater. Interfaces* **2018**, *10* (35), 29730−29740.
(30) Xu, Y.; Li, Y.; Hua, W.; Zhang, A. M.; Bao, J. J. Light-Weight Silver Plating Foam and Carbon Nanotube Hybridized Epoxy Composite Foams with Exceptional Conductivity and Electromagnetic Shielding Property. *ACS Appl. Mater. Interfaces* **2016**, *8* (36), 24131−24142.
(31) Ma, H. F.; Liu, Z. B.; Wu, L.; Wang, Y. H.; Wang, X. X. Study of a pre-treatment process for electroless copper plating on ceramics. *Thin Solid Films* **2011**, *519* (22), 7860−7863.
(32) Huang, B.; Gan, W. P.; Zhou, J.; Li, Y. F.; Lin, T.; Liu, X. G. Factors Affecting the Morphology of Pb-Based Glass Frit Coated with Ag Material Prepared by Electroless Silver Plating. *J. Electron. Mater.* **2014**, *43* (5), 1326−1334.
(33) Cui, C. H.; Yan, D. X.; Pang, H.; Jia, L. C.; Xu, X.; Yang, S.; Xu, J. Z.; Li, Z. M. A high heat-resistance Bioplastic foam with efficient electromagnetic interference shielding. *Chem. Eng. J.* **2017**, *323*, 29−36.
(34) Xu, Y. D.; Yang, Y. Q.; Yan, D. X.; Duan, H. J.; Zhao, G. Z.; Liu, Y. Q. Flexible and conductive polyurethane composites for electromagnetic shielding and printable circuit. *Chem. Eng. J.* **2019**, *360*, 1427−1436.
(35) Xu, Y. F.; Qian, K. P.; Deng, D. M.; Luo, L. Q.; Ye, J. H.; Wu, H. M.; Miao, M.; Feng, X. Electroless deposition of silver nanoparticles on cellulose nanofibrils for electromagnetic interference shielding films. *Carbohydr. Polym.* **2020**, *250*, 116915.
(36) Lutkenhaus, J. A radical advance for conducting polymers. *Science* **2018**, *359* (6382), 1334−1335.
(37) Geleil, A. S.; Hall, M. M.; Shelby, J. E. Hollow glass microspheres for use in radiation shielding. *J. Non-Cryst. Solids* **2006**, *352* (6−7), 620−625.
(38) Ashton-Patton, M. M.; Hall, M. M.; Shelby, J. E. Formation of low density polyethylene/hollow glass microspheres composites. *J. Non-Cryst. Solids* **2006**, *352* (6−7), 615−619.
(39) Yu, Z. Y.; Gao, Y. F.; Di, X.; Luo, H. J. Cotton modified with silver-nanowires/polydopamine for a wearable thermal management device. *RSC Adv.* **2016**, *6* (72), 67771−67777.
(40) Li, H. T.; Fu, C. J.; Chen, N.; Zhang, T.; Liu, J. M.; Du, G. P.; Ren, L. L.; Zeng, X. L.; Sun, R. Ice-templated assembly strategy to construct three-dimensional thermally conductive networks of BN nanosheets and silver nanowires in polymer composites. *Compos. Commun.* **2021**, *25*, 100601.
(41) Zeng, Z. H.; Wu, T. T.; Han, D. X.; Ren, Q.; Siqueira, G.; Nyström, G. Ultralight, Flexible, and Biomimetic Nanocellulose/Silver Nanowire Aerogels for Electromagnetic Interference Shielding. *ACS Nano* **2020**, *14* (3), 2927−2938.
(42) Fu, B. Q.; Ren, P. G.; Guo, Z. Z.; Du, Y. L.; Jin, Y. L.; Sun, Z. F.; Dai, Z.; Ren, F. Construction of three-dimensional interconnected graphene nanosheet network in thermoplastic polyurethane with highly efficient electromagnetic interference shielding. *Composites, Part B* **2021**, *215*, 108813.
(43) Shen, Y. K.; Lin, Z. Q.; Liu, X. B.; Zhao, T.; Zhu, P. L.; Zeng, X. R.; Hu, Y. G.; Sun, R.; Wong, C. P. Robust and flexible silver-embedded elastomeric polymer/carbon black foams with outstanding electromagnetic interference shielding performance. *Compos. Sci. Technol.* **2021**, *213*, 108942.
(44) Ganguly, S.; Ghosh, S.; Das, P.; Das, T. K.; Ghosh, S. K.; Das, N. C. Poly(N-vinylpyrrolidone)-stabilized colloidal graphene-reinforced poly(ethylene-co-methyl acrylate) to mitigate electromagnetic radiation pollution. *Polym. Bull.* **2020**, *77* (6), 2923−2943.
(45) Shi, H. G.; Zhao, H. B.; Liu, B. W.; Wang, Y. Z. Multifunctional Flame-Retardant Melamine-Based Hybrid Foam for Infrared Stealth, Thermal Insulation, and Electromagnetic Interference Shielding. *ACS Appl. Mater. Interfaces* **2021**, *13* (22), 26505−26514.
(46) Jiang, D. X.; Tian, S.; Li, H. J.; Du, Z. W.; Liu, T.; Yan, D. K.; Zhou, L.; Bai, S.; Qiang, X. F. Lightweight HfC nanowire-carbon fiber/graphene aerogel composites for high-efficiency electromagnetic interference shielding. *Carbon* **2024**, *219*, 118788.
(47) Li, S.; Du, Y. K.; Ye, H. R.; Wu, J. M.; Wang, Y.; Liang, Y. Y.; Zhu, M. W.; Lam, S. S.; Liu, C. W.; Li, J. Z.; Xia, C. L. All-Natural Self-Bonded Biocomposite Providing Superior Electromagnetic Interference Shield Performance with Effective Absorption. *Adv. Funct. Mater.* **2024**, *34*, 2406282.
(48) Guan, Q. F.; Han, Z. M.; Yang, K. P.; Yang, H. B.; Ling, Z. C.; Yin, C. H.; Yu, S. H. Sustainable Double-Network Structural Materials for Electromagnetic Shielding. *Nano Lett.* **2021**, *21* (6), 2532−2537.

https://doi.org/10.1021/acsomega.5c00148
ACS Omega 2025, 10, 11516−11524